

Is the FeO_2^- Anion Bent or Linear?

Zhen Hua Li,* Yu Gong, Kangnian Fan, and Mingfei Zhou*

Department of Chemistry, Shanghai Key Laboratory of Molecular Catalysts and Innovative Materials, Advanced Materials Laboratory, Fudan University, Shanghai 200433, People's Republic of China

Received: August 5, 2008; Revised Manuscript Received: October 16, 2008

FeO_2^- anions were produced by co-condensation of laser-ablated iron atoms and electrons with dioxygen in excess argon at 6 K. A photosensitive absorption at 870.6 cm^{-1} is assigned to the antisymmetric OFeO stretching vibration (ν_3) of the inserted FeO_2^- anion trapped in solid argon. On the basis of the observed ν_3 vibrational frequencies for Fe^{16}O_2 and Fe^{18}O_2 , the anion is estimated to be linear. Due to the severe symmetry-breaking problems of the reference wave function, calculations with single-reference methods, including various DFT and post-HF methods, are unreliable for this molecule. However, the state-averaged multireference MRCI method, which incorporates both dynamical and nondynamical correlations, predicted that the anion has a linear doublet ground state, consistent with the experimental observations.

Introduction

The interaction of iron with oxygen is of great chemical interest. There have been many investigations on the reaction products formed by iron and oxygen. The spectra, structures, and bonding of the neutral iron oxides, particularly the monoxide and dioxide molecules, have received considerable attention both experimentally and theoretically.^{1–14} Iron oxide anions have also gained much attention.^{10,15–26} Collision-induced dissociation studies of iron oxide cluster anions show that small mononuclear anions such as FeO_2^- and FeO_3^- are the stable building blocks of the larger iron oxide clusters.²⁰ Anion photoelectron spectroscopic investigations on the iron oxide anions indicate that the FeO_2^- anion has an inserted OFeO structure similar to the FeO_2 neutral, and other isomers involving weakly bonded Fe–O₂ complexes were not observed in the gas phase.^{10,16,17} Theoretical calculations also predict that the inserted dioxide anion is the most stable isomer on the potential energy surfaces of FeO_2^- .^{21–25} There is no experimental report on the vibrational spectra of the iron oxide anions.

The electronic structure and geometry of the ground state of the FeO_2^- anion remain unclear. Earlier ab initio calculations at the HF, MP2, and CCSD(T) levels of theory with the TZV* basis set predict that the FeO_2^- anion has a linear sextet ground state,²² whereas density functional theory (DFT) calculations with generalized gradient approximation for the exchange-correlation potential show that the FeO_2^- anion has several closely spaced stable states, the ground state is a bent $^4\text{B}_2$ state followed by $^4\text{A}_2$ (+0.05 eV), $^2\text{A}_1$ (+0.06 eV), $^2\text{B}_1$ (+0.12 eV), and $^6\text{A}_1$ (+0.35 eV) states.²⁴ Similar discrepancy has also been found for the isoelectronic CoO_2 molecule: BPW91 calculations²⁴ predict a bent structure with an $^2\text{A}_1$ ground state, whereas ab initio CASSCF calculations²⁷ predict a linear structure with an $^2\Delta_g$ ground state, and CCSD(T)¹⁴ and BILYP^{14,28} calculations predict a linear $^6\text{A}_1$ (the final structure seems to be optimized starting from a bent structure) ground state. However, experimental data for CoO_2 indicate that it is linear with a doublet spin state.^{27,29} Theoretical calculations on PtO_2^+ found that DFT methods predict the inserted PtO_2^+ molecule to be bent while

multireference methods predict that it is linear with a doublet spin state.³⁰ From the results of CoO_2 and PtO_2^+ , it seems that the isoelectronic FeO_2^- anion might be linear as well.

It appears that many disagreements were found in the literature for FeO_2^- . Hence, we performed a combined matrix isolation infrared spectroscopic and systematic theoretical investigation on the FeO_2^- anion. Both the experimental observations and our best theoretical results indicate that the FeO_2^- anion has a doublet ground state with a linear geometry.

Experimental and Computational Details

The experimental setup for pulsed laser-ablation and matrix isolation infrared spectroscopic investigation has been described in detail previously.³¹ Briefly, the 1064 nm fundamental of a Nd:YAG laser (Continuum, Minilite II, 10 Hz repetition rate and 6 ns pulse width) was focused onto a rotating iron metal target through a hole in a CsI window cooled normally to 6 K by means of a closed-cycle helium refrigerator (ARS, 202N). The ablated iron atoms and electrons were codeposited with O₂ in excess argon onto the CsI window. In general, matrix samples were deposited for 1 h at a rate of approximately 4 mmol/h. The O₂/Ar mixtures were prepared in a stainless steel vacuum line, using standard manometric technique. O₂ (Shanghai BOC, 99.95%) and isotopic ¹⁸O₂ (ISOTEC, 99%) were used without further purification. The infrared absorption spectra of the resulting samples were recorded on a Bruker IFS 66V spectrometer at 0.5 cm⁻¹ resolution between 4000 and 450 cm⁻¹, using a liquid nitrogen cooled HgCdTe (MCT) detector. Samples were annealed to different temperatures and cooled back to 6 K for spectral acquisition. Selected samples were subjected to 355 nm laser irradiation.

For theoretical calculations, we have chosen two groups of methods. The first group is single-reference-based methods including MP2,³² MP3,³³ MP4,³⁴ CCSD,³⁵ CCSD(T),³⁶ and DFT. Several well-calibrated DFT methods (BLYP,^{37,38} OLYP,^{37,39} BPW91,^{37,40} B97-2,⁴¹ O3LYP,^{38,39,42} B3LYP,^{37,38,43} B3PW91,^{37,40,44} TPSSSTPSS,⁴⁵ BILYP,⁴⁶ and BHandHLYP)^{37,38,47} available in the Gaussian 03 software package were employed,⁴⁸ which were proven to give good results for transition metal-containing compounds.^{49,50} The second group involves the CASSCF⁵¹ and internally contracted MRCI methods.⁵² The 6-311+G(2df) basis

* Corresponding author. E-mail: lizhenhua@fudan.edu.cn (Z.H.L.) and mzhzhou@fudan.edu.cn (M.Z.).

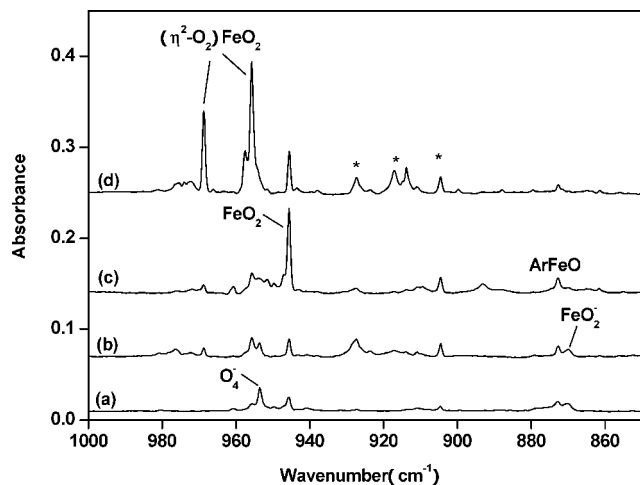


Figure 1. Infrared spectra in the 1000–850 cm^{-1} region from codeposition of laser evaporated iron atoms with 1.0% O_2 in argon: (a) 1 h of sample deposition at 6 K, (b) after 20 K annealing, (c) after 10 min of 355 nm irradiation, and (d) after 30 K annealing. The asterisks denoted absorptions are due to some unknown Fe_xO_y clusters.

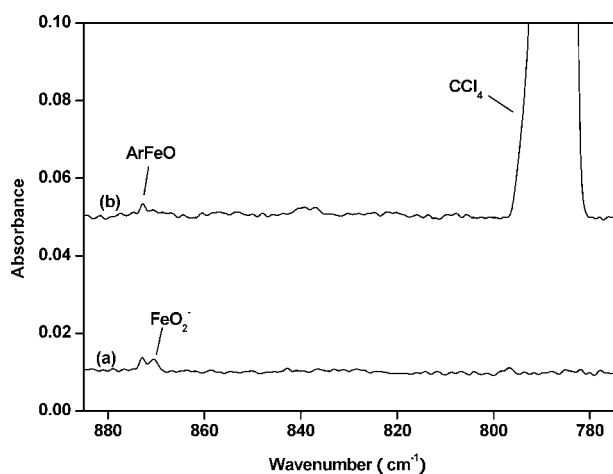


Figure 2. Infrared spectra in the 885–775 cm^{-1} region from codeposition of laser-evaporated Fe atoms with different gas mixtures. Spectra were taken after 1 h of sample deposition: (a) 1% O_2 in argon and (b) 1% O_2 + 0.1% CCl_4 in argon.

set is used for O and the aug-cc-pVTZ-NR basis set is employed for Fe (NR stands for nonrelativistic).⁵³ The integral grid used for DFT calculations is a pruned (99 590) grid. To consider relativistic effect, the relativistic aug-cc-pVTZ-DK basis set is used for Fe.⁵³ The scalar relativistic effect was taken into account by using the second-order Douglas–Kroll–Hess (DKH) approach.⁵⁴

The calculations with the first group methods were performed with Gaussian 03,⁴⁸ while the state-averaged CASSCF (SA-CAS) and MRCI (SA-MRCI) calculations were performed with Molpro 2002.6.⁵⁵ The latter includes an active space with the 3d and 4s orbitals of Fe and 2p orbitals of O. Tight geometry convergence criterion is used due to the floppiness of the potential energy surface (PES) with respect to the bending of the OFeO bond angle. Harmonic vibrational analyses were performed analytically for all nonrelativistic DFT and MP2 calculations. All DFT and post-HF calculations were performed with spin unrestricted HF or Kohn–Sham orbitals.

To calculate spin–orbit eigenstates, SA-MRCI energies were used as the unperturbed energies (the diagonal elements) of the spin–orbit matrix, while the off-diagonal spin–orbit matrix elements were calculated by using the SA-CAS wave functions

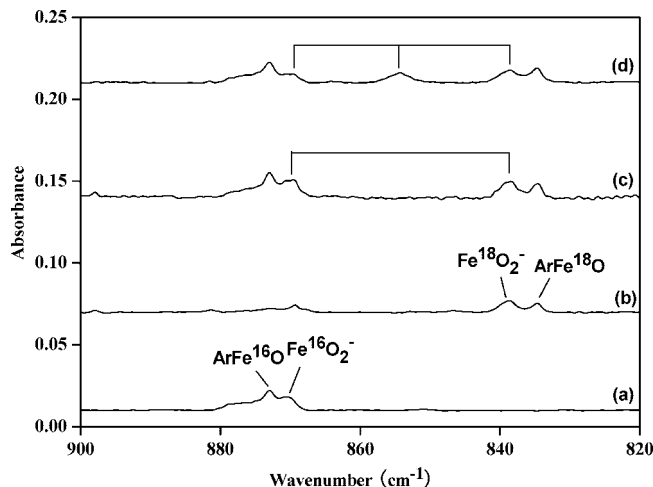


Figure 3. Infrared spectra in the 900–820 cm^{-1} region from codeposition of laser-evaporated iron with O_2 in excess argon. Spectra were taken after 1 h of sample deposition at 6 K: (a) 1.0% $^{16}\text{O}_2$, (b) 1.0% $^{18}\text{O}_2$, (c) 0.5% $^{16}\text{O}_2$ + 0.5% $^{18}\text{O}_2$, and (d) 0.25% $^{16}\text{O}_2$ + 0.5% $^{18}\text{O}_2$.

with a smaller basis set (6-31+G(d) for O and 6-31G(d) for Fe). The spin–orbit operator used to calculate the spin–orbit matrix elements is the Breit–Pauli operator. The spin–orbit matrix was then diagonalized to give spin–orbit eigenstates.

Results and Discussion

The anions were produced by the technique of laser ablation, which has been proven to be a powerful method to produce reactive intermediates and free radicals for gas phase jet studies as well as low-temperature matrix isolation studies.⁵⁶ Laser ablation of the metal target produces metal atoms as well as electrons, and as a result, anions can be formed by electron capture of the neutral molecules during sample deposition. Anions usually have small electron affinities (less than 4 eV) and are photosensitive. Thus electrons can be easily detached from them by visible or ultraviolet irradiation. As laser ablation of the metal target produces a plume of radiation, and the samples were deposited with concurrent irradiation, no anion species were reported in the previous investigations on the reactions of laser-ablated iron with oxygen.^{11,13} In the present experiments, we employ quite low laser energy (3–5 mJ/pulse) to minimize the plume of irradiation and to favor the trapping of charged species in solid argon.

Figure 1 shows the spectra in the 1000–850 cm^{-1} region from codeposition of laser-ablated iron atoms and electrons with 1.0% O_2 in argon. The absorptions due to O_3 (1039.8 cm^{-1} , not shown), O_4^- (953.8 cm^{-1}), and O_4^+ (1118.7 cm^{-1} , not shown) that are common to other metal reactions with O_2 were observed.⁵⁷ In addition, product absorptions at 872.8, 945.8, 797.0, and 870.6 cm^{-1} were observed after sample deposition at 6 K. The 945.8 and 797.0 cm^{-1} absorptions are due to the antisymmetric (ν_3) and symmetric (ν_1) stretching vibrations of the inserted FeO_2 molecule.¹¹ The 872.8 cm^{-1} absorption was previously assigned to the FeO absorption,¹¹ but recent investigation in this group indicates that it should be regarded as ArFeO isolated in solid argon.⁵⁹ The 870.6 cm^{-1} absorption was not observed in the previous experiments employing relatively high ablation laser energy.¹¹ This absorption remains almost unchanged upon sample annealing to 25 K, but it was destroyed when the sample was subjected to 355 nm laser irradiation and its intensity cannot be recovered on subsequent sample annealing to high temperatures. Strong absorptions at 968.8 and 955.9

TABLE 1: Relative Energies (eV) Calculated by Various Methods^a

method	<i>C</i> _{2v}					<i>D</i> _{∞h}			
	² A ₁	² B ₁	⁴ A ₂	⁴ B ₂	⁶ A ₁	² Δ _g ^b	² Σ _g ⁺	⁴ Π _g ^b	⁶ Σ _g ⁺
BLYP	0.00	0.04	0.08	0.04	0.48	0.11	0.42	0.24	0.73
B3LYP	0.34	0.36	0.01	0.00	0.11	0.41	0.74	0.08	0.16
B1LYP	0.45	0.46	0.00	— ^c	0.00	0.50	0.88	0.03	0.02
BHandHLYP	1.51	1.51	— ^c	— ^c	— ^c	1.52	1.95	0.24	0.00
OLYP	0.22	0.32	0.02	0.00	0.14	0.44	0.56	0.19	0.31
O3LYP	0.46	0.51	0.03	0.02	0.00	0.60	0.77	0.14	0.06
BPW91	0.08	0.15	0.06	0.00	0.38	0.23	0.47	0.23	0.63
B3PW91	0.46	0.48	0.01	0.00	0.04	0.54	0.82	0.09	0.09
B97-2	0.46	0.48	0.05	0.05	0.00	0.56	0.80	0.12	0.00
TPSSTPSS	0.09	0.12	0.03	0.00	0.42	0.18	0.60	0.17	0.61
MP2	0.38	0.41	1.37	1.28	— ^c	0.48	1.05	2.19	0.00
MP3	— ^c	— ^c	3.44	2.12	— ^c	2.01	2.86	1.38	0.00
CCSD	1.15	1.15	— ^d	— ^c	— ^c	1.17	1.70	0.42	0.00
CCSD(T) ^e	0.45	0.46	— ^d	— ^c	— ^c	0.53	0.87	0.39	0.00

^a All energies are relative to the electronic ground state (marked bold) at that level of theory. The basis sets used are 6-311+G(2df) for O and aug-cc-pVTZ-NR for Fe. ^b A few occupied orbitals have undefined symmetry. The symmetry of the wave function was judged from HF orbital pictures. ^c The final optimized geometry is a *D*_{∞h} structure. ^d Geometry optimization could not converge due to discontinuity in the potential energy surface. ^e Single point calculations on CCSD optimized geometry.

TABLE 2: Harmonic Vibrational Frequencies (cm⁻¹) of the Antisymmetric Stretching Mode of FeO₂⁻. Bold Value Indicates That the Corresponding Structure is a Transition State^a

method	<i>C</i> _{2v}					<i>D</i> _{∞h}			
	² A ₁	² B ₁	⁴ A ₂	⁴ B ₂	⁶ A ₁	² Δ _g ^b	² Σ _g ⁺	⁴ Π _g ^b	⁶ Σ _g ⁺
BLYP	959.7	961.6	872.9	879.5	778.8	963.1	945.0	843.8	802.8
B3LYP	993.6	997.5	884.8	883.5	850.1	1002.5	984.6	797.3	854.3
B1LYP	973.2	985.8	856.3	— ^c	859.0	997.6	987.3	712.1	861.2
BHandHLYP	1100.6	1122.2	— ^c	— ^c	— ^c	1002.7	1018.1	2166.6	916.5
OLYP	956.7	959.4	874.9	886.1	789.3	957.0	947.2	829.5	811.0
O3LYP	971.9	979.1	881.2	879.4	830.3	978.2	969.7	806.5	839.4
BPW91	975.2	980.5	891.0	898.7	804.6	981.0	961.3	858.1	826.2
B3PW91	876.3	1009.6	895.8	895.3	867.6	1014.4	996.0	800.4	871.8
B972	994.1	997.1	882.3	874.7	850.0	997.5	987.9	777.6	850.6
TPSSTPSS	989.2	991.7	899.2	905.0	817.4	993.2	973.8	864.6	838.5
MP2	3751.1	1103.1	678.4	997.1	— ^c	1054.3	983.3	2649.4i	847.3
MP3	— ^c	— ^c	170.4	— ^d	— ^c	1009.5	971.1	19452.2i	940.7
CCSD	— ^d	— ^e	— ^d	— ^c	— ^c	1022.6	992.4	696.0	894.9
EXP						870.6			

^a The basis sets used are 6-311+G(2df) for O and aug-cc-pVTZ-NR for Fe. ^b A few occupied orbitals have undefined symmetry. The symmetry of the wave function was judged from HF or Kohn–Sham orbital pictures. ^c A final linear *D*_{∞h} structure was optimized. ^d HF wave function breaks symmetry during the numerical evaluation of Hessian matrix and it produces discontinuity in PES. ^e Geometry optimization could not converge due to the discontinuity in PES.

cm⁻¹ together with some unknown weak absorptions at 927.4, 917.1, 913.8, and 904.6 cm⁻¹ (marked with asterisks in Figure 1) appeared on sample annealing. The 955.9 cm⁻¹ absorption was previously assigned to the O–O stretching (ν_1) mode of cyclic Fe(O₂), this absorption together with the 968.8 cm⁻¹ absorption was reassigned to the symmetric and antisymmetric FeO₂ stretching modes of the side-on bonded peroxy–iron dioxide complex, (η^2 -O₂)FeO₂.⁵⁸ The end-on bonded (η^1 -O₂)FeO₂ complex, which exhibits absorptions at 1204.5, 975.3, and 871.6 cm⁻¹,⁵⁸ is not observed here due to large sample scan times. As has been discussed, the (η^1 -O₂)FeO₂ absorptions are very photosensitive and decreased quickly with increasing the sample scan times, during which the sample was irradiated by the light emitted from the IR source.⁵⁸

One experiment was done with CCl₄ doped to serve as an electron trap.⁶⁰ As shown in Figure 2, the 870.6 cm⁻¹ absorption was eliminated when 0.1% CCl₄ was doped. One experiment was performed with 1.0% ¹⁸O₂ in argon and all the product absorptions were shifted. Similar experiments were done with the 0.5% ¹⁶O₂ + 0.5% ¹⁸O₂, and 0.25% ¹⁶O₂ + 0.5% ¹⁶O¹⁸O + 0.25% ¹⁸O₂ mixed samples. The spectra in the 900–820 cm⁻¹ region with different isotopic samples are shown in Figure 3.

The weak band at 870.6 cm⁻¹ was observed on sample deposition and destroyed on 355 nm laser photolysis. This band was not observed in the previous thermal iron atom and oxygen reaction experiments, which suggests that the band is due to a charged species. The removal of this absorption from identical experiment upon doping with the electron trapping molecule adds strong support to the identification as an anion. The 870.6 cm⁻¹ band shifted to 839.7 cm⁻¹ with ¹⁸O₂. The ¹⁶O/¹⁸O isotopic frequency ratio of 1.0368 is characteristic of an antisymmetric OFeO stretching vibration. In the mixed ¹⁶O₂ + ¹⁸O₂ experiment, only the pure isotopic counterparts were presented, while a triplet was observed in the ¹⁶O₂ + ¹⁶O¹⁸O + ¹⁸O₂ experiment (Figure 3), which indicate that two equivalent oxygen atoms are involved. Therefore, we assign the 870.6 cm⁻¹ band to the antisymmetric stretching vibration of the FeO₂⁻ anion. The ¹⁶O/¹⁸O isotopic frequency ratio of the antisymmetric stretching vibration (1.0368) implies that the FeO₂⁻ anion is *linear*. This ratio is lower than that of the neutral FeO₂ molecule (1.0380). The bond angle of neutral FeO₂ was determined from the oxygen and iron isotopic frequencies to be 150(±10)°.¹¹

To verify whether the FeO₂⁻ anion is linear or bent and to determine its electronic ground state, quantum chemical calcula-

TABLE 3: IR Intensities (km/mol) of the Antisymmetric Stretching Mode of FeO₂^{-a}

method	<i>C</i> _{2v}					<i>D</i> _{∞h}			
	² A ₁	² B ₁	⁴ A ₂	⁴ B ₂	⁶ A ₁	² Δ _g ^b	² Σ _g ⁺	⁴ Π _g ^b	⁶ Σ _g ⁺
BLYP	246.1	236.2	329.4	277.8	235.9	267.4	475.9	354.2	393.3
B3LYP	273.8	290.5	354.3	334.8	367.5	285.5	602.1	105.1	458.2
B1LYP	192.8	265.6	238.8	— ^c	407.5	258.8	626.7	0.7	467.9
BHandHLYP	1829.7	777.4	— ^c	— ^c	— ^c	163.8	720.6	-229402.9	554.5
OLYP	243.5	215.5	333.3	271.8	277.5	254.1	490.2	325.5	416.3
O3LYP	235.0	248.7	369.5	354.3	356.4	249.9	560.2	199.3	457.2
BPW91	230.9	233.7	337.8	291.9	245.2	265.8	479.0	354.9	400.1
B3PW91	37.3	284.6	356.9	336.4	483.2	281.4	602.5	98.2	478.0
B972	263.9	274.9	347.0	313.8	494.2	250.9	612.9	59.2	496.8
TPSSTPSS	245.4	245.4	353.3	324.0	250.9	271.1	499.0	337.9	392.1
MP2	— ^d	360.2	979.1	1566.1	— ^c	36.0	1216.4	-935476.2	671.9
MP3	— ^c	— ^c	1422.8	— ^e	— ^c	547.1	155.5	— ^d	636.8
CCSD	— ^e	— ^f	— ^e	— ^c	— ^c	213.8	653.8	190.3	596.9

^a Bold values indicate that the corresponding structure is a transition state. The basis functions used are 6-311+G(2df) for O and aug-cc-pVTZ-NR for Fe. ^b A few occupied orbitals have undefined symmetry. The symmetry of the wave function was judged from HF or Kohn–Sham orbital pictures. ^c A final linear *D*_{∞h} structure was optimized. ^d IR intensity too large to be printed out by the Gaussian 03 program. ^e HF wave function breaks symmetry during the numerical evaluation of Hessian matrix and it produces discontinuity in PES. ^f Geometry optimization could not converge due to the discontinuity in PES.

TABLE 4: Douglas–Kroll–Hess 2nd Order Scalar Relativistic Calculations for Several States of the Bent Structure at the DFT Level^a

method	² A ₁			⁴ B ₂				⁶ A ₁		
	Δ <i>E</i> (eV)	<i>R</i> _{FeO} (Å)	<i>A</i> _{OFeO} (deg)	Δ <i>E</i> (eV)	<i>R</i> _{FeO} (Å)	<i>A</i> _{OFeO} (deg)	<i>ν</i> ₃ (cm ⁻¹)	Δ <i>E</i> (eV)	<i>R</i> _{FeO} (Å)	<i>A</i> _{OFeO} (deg)
BLYP	0.00	1.620	144.4	0.12	1.642	125.3	895.5	0.59	1.717	141.9
B3LYP	0.22	1.608	149.7	0.00	1.647	142.8	898.8	0.10	1.702	152.6
OLYP	0.16	1.601	140.4	0.00	1.629	124.9	902.8	0.18	1.705	143.4
O3LYP	0.36	1.597	143.0	0.03	1.640	140.3	893.0	0.00	1.698	149.9
BPW91	0.00	1.606	142.7	0.00	1.632	127.2	913.2	0.40	1.703	141.5
B3PW91	0.34	1.598	148.0	0.00	1.637	141.3	911.4	0.02	1.692	152.2
B97-2	0.35	1.596	146.3	0.13	1.622	126.9	931.6	0.00	1.699	180.0
TPSSTPSS	0.00	1.609	145.8	0.01	1.633	129.3	920.6	0.44	1.702	143.4

^a All energies are relative to the electronic ground state (marked bold) at that level of theory. The basis sets used are the relativistic aug-cc-pVTZ-DK basis set for Fe and the nonrelativistic 6-311+G(2df) basis set for O.

TABLE 5: Key Geometry Parameters of FeO₂⁻ from Nonrelativistic DFT Calculations^a

method	² A ₁		⁴ B ₂		⁶ A ₁	
	<i>R</i> _{FeO} (Å)	<i>A</i> _{OFeO} (deg)	<i>R</i> _{FeO} (Å)	<i>A</i> _{OFeO} (deg)	<i>R</i> _{FeO} (Å)	<i>A</i> _{OFeO} (deg)
BLYP	1.625	142.4	1.652	128.6	1.723	141.6
B3LYP	1.615	147.2	1.654	142.9	1.707	151.9
OLYP	1.607	139.5	1.638	126.7	1.712	143.0
O3LYP	1.603	141.4	1.647	140.4	1.704	149.1
BPW91	1.611	141.2	1.640	129.3	1.709	141.2
B3PW91	1.604	145.6	1.644	141.8	1.698	151.5
B97-2	1.603	144.2	1.650	144.6	1.705	174.6
TPSSTPSS	1.614	143.6	1.640	132.8	1.708	142.4

^a The basis sets used are aug-cc-pVTZ-NR for Fe and 6-311+G(2df) for O.

tions were performed. We first optimize the geometry of FeO₂⁻ with the single-reference-based methods for several states, and the results are listed in Table 1. As can be seen from Table 1, the electronic ground state of FeO₂⁻ depends strongly on the method used. Among the DFT methods used, only BHandHLYP predicts a linear ground state structure, while all other methods predict a bent ground state structure. Only the BLYP method predicts that the doublet ²A₁ state is the electronic ground state, while all other methods prefer high spin state to be the electronic ground state. The post-HF methods including MP2, MP3, CCSD, and CCSD(T) all predict that the linear ⁶Σ_g⁺ state is the ground state. Cao et al. have studied the bent ²A₁, linear ⁴B₂, and ⁶A₁ states (under the *C*_{2v} point group notation) using post-

HF methods.²² They also concluded that the sextet state is the ground state.

The harmonic vibrational frequencies and IR intensities of the *ν*₃ mode calculated at various levels are listed in Tables 2 and 3, respectively. Compared to the experimental vibrational frequency, BHandHLYP, the only DFT method that predicts a linear electronic ground state (sextet), gives a reasonable *ν*₃ vibrational frequency of 916.5 cm⁻¹. However, the same method predicts a very high *ν*₃ vibrational frequency of 2166.6 cm⁻¹ with an unphysical intensity of -229402.9 km/mol for the linear quartet state. An unusually high IR intensity for the bending ²A₁ state is also obtained with the BHandHLYP method. Although all the single-reference post-HF methods predict a linear ⁶Σ_g⁺ ground state, the *ν*₃ vibrational frequency for this state strongly depends on the level of theory used: MP2 predicts a value of 847.3 cm⁻¹; MP3 predicts a value of 940.7 cm⁻¹; and CCSD predicts a value of 894.9 cm⁻¹. This is in disagreement with the general trend that a higher level correlation method would give lower vibrational frequencies.⁶¹ For the other states, these three methods also give controversial results. MP2 gives a very high vibrational frequency of 3751.1 cm⁻¹ for the ²A₁ state, and an imaginary one (2649.4i cm⁻¹) with an unphysical IR intensity (-935476.2 km/mol) for the linear ⁴Π_g state. At the MP3 level, the bent ⁴A₂ state has a very low vibrational frequency of 170.4 cm⁻¹. Apparently, the results predicted by the above-mentioned single-reference-based methods are highly doubtful.

TABLE 6: $\langle S^2 \rangle$ Values of the HF/Kohn–Sham Wave Function^a

method	C_{2v}					$D_{\infty h}$			
	2A_1	2B_1	4A_2	4B_2	6A_1	$^2\Delta_g$	$^2\Sigma_g^+$	$^4\Pi_g$	$^6\Sigma_g^+$
BLYP	0.77	0.78	3.78	3.78	8.77	0.79	0.75	3.82	8.77
B3LYP	0.81	0.82	3.85	3.85	8.79	0.86	0.76	3.96	8.78
B1LYP	0.85	0.86	3.91	— ^a	8.79	0.91	0.77	4.04	8.79
BHandHLYP	1.09	1.10	— ^a	— ^a	— ^a	1.17	0.80	4.47	8.81
OLYP	0.78	0.80	3.80	3.81	8.77	0.83	0.76	3.85	8.77
O3LYP	0.80	0.83	3.84	3.84	8.78	0.87	0.77	3.92	8.78
BPW91	0.77	0.78	3.79	3.78	8.77	0.79	0.76	3.82	8.77
B3PW91	0.81	0.82	3.85	3.86	8.78	0.86	0.77	3.97	8.78
B97-2	0.83	0.85	3.87	3.87	8.79	0.90	0.77	3.98	8.79
TPSSPTSS	0.78	0.79	3.79	3.79	8.77	0.81	0.76	3.83	8.77
MP2	1.11	1.20	4.48	4.12	— ^a	1.39	0.90	5.05	8.82
MP3	— ^a	— ^a	5.45	4.21	— ^a	1.72	1.11	5.16	8.82
CCSD	1.42	1.44	— ^b	— ^a	— ^a	1.61	0.97	5.17	8.82
ideal value	0.75	0.75	3.75	3.75	8.75	0.75	0.75	3.75	8.75

^a A final linear $D_{\infty h}$ structure was optimized. ^b Geometry optimization could not converge due to the discontinuity in the PES.

To explore the relativistic effect, we recomputed the bent 2A_1 , 4B_2 , and 6A_1 states using the second-order Douglas–Kroll–Hess (DKH) approach in which the scalar relativistic effects are taken into consideration. The results are presented in Table 4. For comparison, the key geometric parameters optimized by the nonrelativistic DFT methods are listed in Table 5. It can be found that relativistic effects have little effect on the calculated geometries and energetics except for the 4B_2 and 6A_1 states with the B97-2 method. We also performed relativistic harmonic vibrational frequency analysis for the 4B_2 state. The ν_3 vibrational frequencies predicted by the DFT methods are all about 15 cm^{-1} higher than the nonrelativistic values. Obviously, relativistic effects for FeO_2^- are small and cannot account for the discrepancy between the DFT results and the experimental observations.

The single-reference wave functions of the FeO_2^- molecule may suffer from severe symmetry breaking problems. DFT methods generally show better resistance to symmetry breaking.^{62,63} However, all the DFT methods employed here do not provide reliable results. The problems caused by symmetry breaking are even much worse for the post-HF methods. The calculated energy gaps between different states strongly depend on the method used and differ by as much as 2.1 eV (Table 1). The ν_3 vibrational frequency predicted also strongly depends on the method used (Table 2). Abnormal frequencies and unphysical IR intensities are obtained for many states. The large $\langle S^2 \rangle$ values of the HF reference functions indicate that the HF reference wave functions of all states except the sextet states are severely spin contaminated (Table 6). The T1 diagnostic value of the CCSD wave function for the $^2\Delta_g$ state is 0.09, much larger than the normal single-reference/multireference borderline value of 0.02.⁶⁴

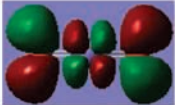
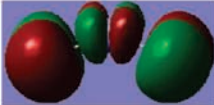
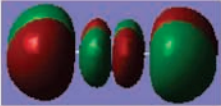
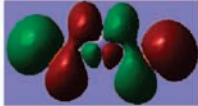
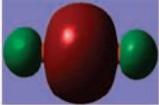
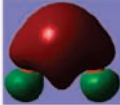
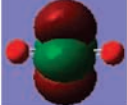
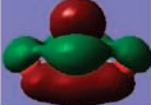
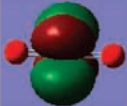
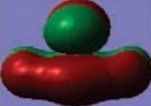
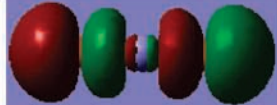
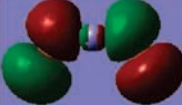




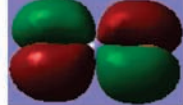

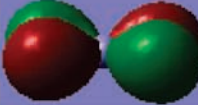
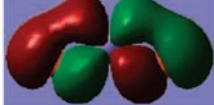
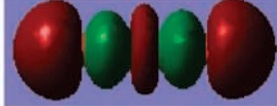
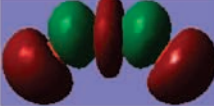
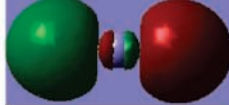
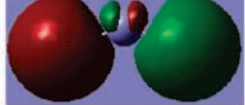
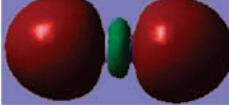

Table 7 lists the valence molecular orbitals of the linear $D_{\infty h}$ and bent C_{2v} structures. For the doublet $^2\Delta_g$ state, the unpaired electron is in the $1\delta_g$ orbitals, which is doubly degenerated. The vibrational bending mode of the linear FeO_2^- will lower the symmetry from $D_{\infty h}$ to C_{2v} and the $^2\Delta_g$ state will split into the 2A_1 and 2B_1 states. The bending may thus create instability in one of the two states or both states. This is the so-called Renner–Teller effect resulting from the coupling between electronic degenerate states and the vibrational bending mode of a linear molecule. The electronic structure calculations of FeO_2^- may also be perturbed by the pseudo-Jahn–Teller effect (PJT), which happens when two noninteracting states, e.g., two states, belong to different irreducible representations may become interacting when the framework of the molecule changes

symmetry.^{65,66} For example, one of the $3\pi_u$ orbitals and one of the $1\delta_g$ orbitals of the linear FeO_2^- anion both belong to the a_1 irreducible representation under C_{2v} point group, and therefore may become interacting when the symmetry is reduced from $D_{\infty h}$ to C_{2v} . If the energies of the two interacting orbitals are close enough, the interaction is strong, which will produce an overall first-order singularity in its force constants along the symmetry-breaking coordinate.⁶⁵

The above discussions indicate that the calculation results with single-reference-based methods are unreliable. Therefore, multireference methods should be used. As discussed above, since both the Renner–Teller effect and the pseudo-Jahn–Teller effect may present, the Jahn–Teller vibronic coupling effects should be considered.⁶⁷ In addition, since FeO_2^- has unpaired electrons and Fe is a transition metal, spin–orbit coupling should also be taken into consideration. Therefore, both vibronic coupling and spin–orbit coupling should be involved in order to obtain reliable energy levels.⁶⁸

We performed state-averaged CASSCF (SA-CAS) calculations including 9 low-lying electronic states (under the C_{2v} point group notation): one 2A_1 , one 2B_1 , three 4A_2 , three 4B_2 , and one 6A_1 . State-averaged MRCI calculations were then performed by using these SA-CAS reference wave functions. A potential energy scan was first performed by symmetrically stretching the FeO bond while fixing the molecule at a linear structure. The equilibrium bond distance for the $^2\Delta_g$ state is determined to be 1.644 Å. The FeO bond is then fixed at 1.644 Å and a second potential energy scan was performed by bending the OFeO angle. The resulting energy profiles are presented in Figures 4 (SA-CAS) and 5 (SA-MRCI). At both the CASSCF and MRCI levels, the electronic ground state is a linear doubly degenerated $^2\Delta_g$ state. This state splits into the 2A_1 and 2B_1 states under the C_{2v} point group notation. The 2A_1 and 2B_1 states are still almost degenerate at the largest bending angle we have considered. This indicates that the Renner–Teller effect is not prominent for the electronic ground state of FeO_2^- at all. For the 4B_2 and 6A_1 excited states, the two methods give qualitatively different results: at the CASSCF level, the energies of the two lowest 4B_2 states decrease rapidly with decreasing the OFeO angle, whereas the highest 4B_2 state increases with decreasing the OFeO angle. The energies of three 4A_2 states increase with decreasing the OFeO angle. Thus, the resulting potential energy minima at the bending geometry for the 4B_2 states are due to the Renner–Teller effect. At the MRCI level, the three 4B_2 states obviously have two avoid-crossing points at OFeO bond angles of around 140° and 160° . In addition, the linear $^6\Sigma_g^+$ state (6A_1

TABLE 7: Valence Molecular Orbitals and Their Irreducible Representations for the Linear FeO_2^- Under the $D_{\infty h}$ and C_{2v} Point Group Notation (in Parentheses) with the C_2 Axis Perpendicular to the Paper Plane and the y Axis Along the Molecular Framework and for the Bent FeO_2^- Under the C_{2v} Point Group Notation with the yz Symmetry Plane in the Paper Plane^a

Linear $D_{\infty h}$ Structure		Bent C_{2v} Structure	
$2\pi_g$ ($2a_2$)		$2a_2$	
$2\pi_g$ ($7b_2$)		$7b_2$	
$7\sigma_g$ ($11a_1$)		$11a_1$	
$1\delta_g$ ($10a_1$)		$10a_1$	
$1\delta_g$ ($4b_1$)		$4b_1$	
$5\sigma_u$ ($6b_2$)		$6b_2$	
$3\pi_u$ ($9a_1$)		$9a_1$	
$3\pi_u$ ($3b_1$)		$3b_1$	
$1\pi_g$ ($1a_2$)		$1a_2$	
$1\pi_g$ ($5b_2$)		$5b_2$	
$6\sigma_g$ ($8a_1$)		$8a_1$	
$4\sigma_u$ ($4b_2$)		$4b_2$	
$5\sigma_g$ ($7a_1$)		$7a_1$	

^a The numbering is not the actual order but just for the convenience of discussion.

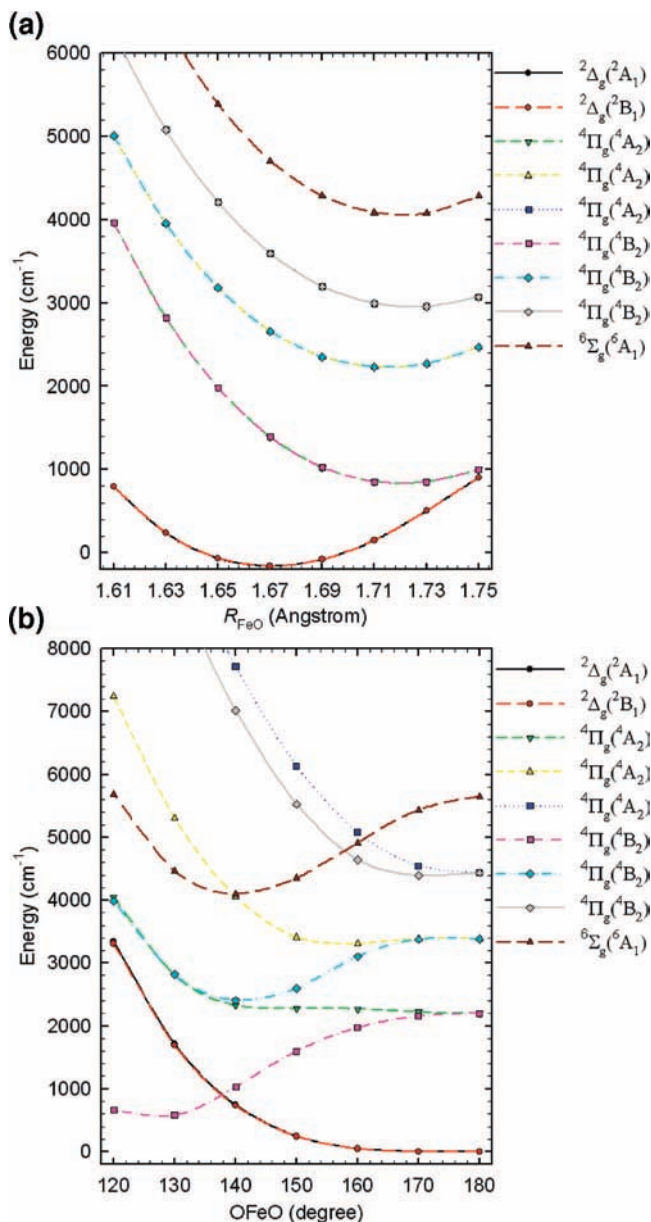


Figure 4. Potential energy profiles of FeO_2^- at the state-averaged CASSCF level without considering spin-orbit coupling effect: (a) by stretching the FeO bond while keeping the molecule linear and (b) by bending the OFeO angle while keeping the FeO bond at 1.644 Å.

under the C_{2v} point group notation) is lower than the $4\Pi_g$ state ($4A_2$ and $4B_2$ under the C_{2v} point group notation) with MRCI, whereas the $6\Sigma_g$ state is the highest one among nine states at the CASSCF level. The results indicate that dynamic correlation is important for the FeO_2^- anion.

After considering the spin-orbit coupling effect, the degenerate states become nondegenerate. The spin-orbit energy profiles (using SA-MRCI energies as unperturbed energies) obtained by symmetrically stretching the FeO bonds and bending the OFeO angle are presented in Figure 6. The spin-orbit coupling constant between the lowest two states is large and the first excited state $2\Delta_{3/2}$ ($2B_1$ in the C_{2v} point group notation) is separated from the electronic ground state $2\Delta_{5/2}$ ($2A_1$ in the C_{2v} point group notation) by 759 cm^{-1} at the linear equilibrium geometry. The second and higher excited states are separated from the first excited state by more than 868 cm^{-1} . Therefore, both the ground state and the first excited state are barely affected by the Renner-Teller and pseudo-Jahn-Teller effects.

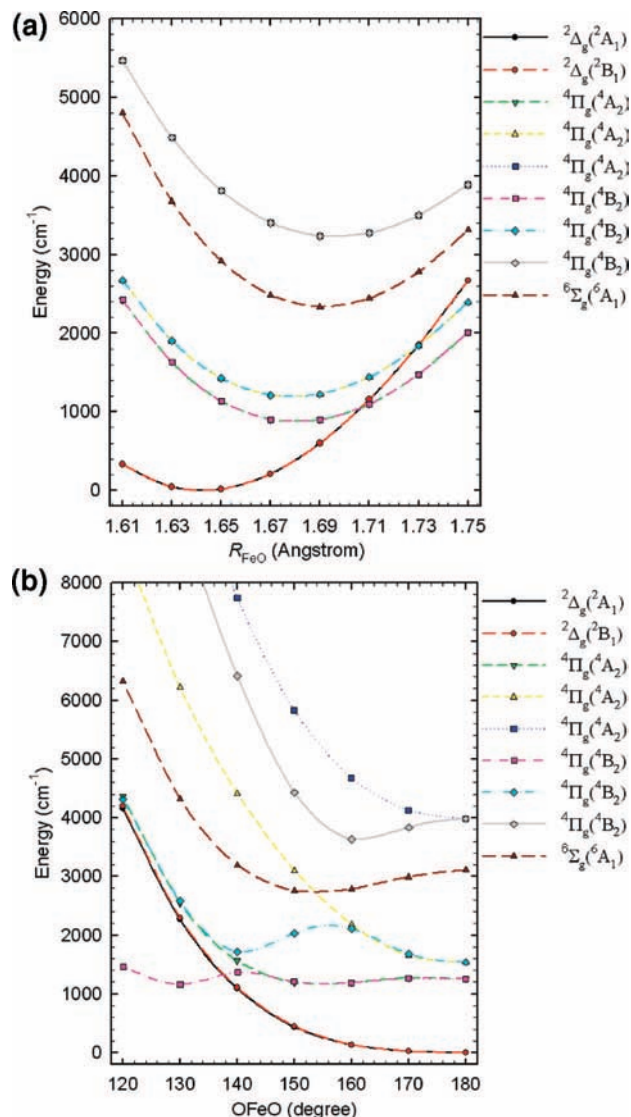


Figure 5. Potential energy profiles of FeO_2^- at the state-averaged MRCI level without considering spin-orbit coupling effect: (a) by stretching the FeO bond while keeping the molecule linear and (b) by bending the OFeO angle while keeping the FeO bond at 1.644 Å.

Both states have a linear equilibrium structure. The energy profiles of the second and higher excited states are greatly affected by the Renner-Teller and pseudo-Jahn-Teller effects and the second and third excited spin states even have multiple minima at bending geometries (one very shallow minimum between 150° and 160° and one at about 130°). Since the electronic ground state of FeO_2^- is barely affected by the Renner-Teller and pseudo-Jahn-Teller effects and is well separated from other excited states, harmonic vibrational frequency analyses at the MRCI level with full valence CASSCF reference wave function (no spin-orbit coupling effect included) give ν_3 vibrational frequencies of 873.8 cm^{-1} for the $2A_1$ state and 884.9 cm^{-1} for the $2B_1$ state, which are in excellent agreement with the experimental value of 870.6 cm^{-1} .

Further Discussion

In the above section, we have demonstrated that all the single-reference-based methods used in the present study are not suitable for the FeO_2^- anion due to the strong multireference character of the molecule and the symmetry-breaking problems in the single-reference wave functions. State-averaged multi-

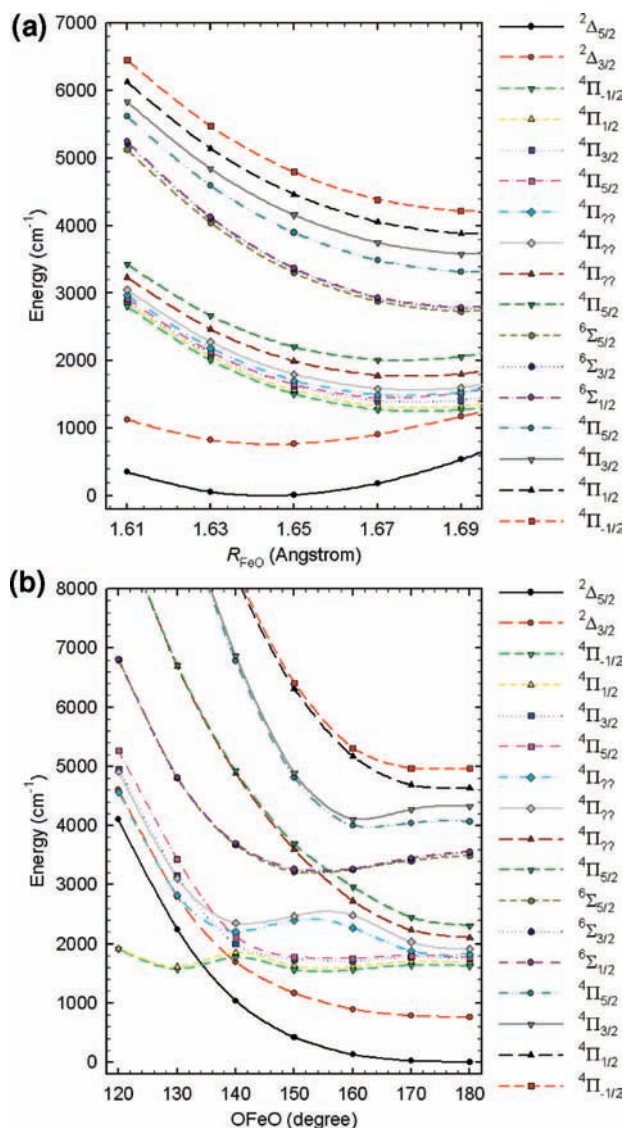


Figure 6. Potential energy profiles of FeO_2^- at the state-averaged MRCI level after considering spin-orbit coupling effect: (a) by stretching the FeO bond while keeping the molecule linear and (b) by bending the OFeO angle while keeping the FeO bond at 1.644 Å.

reference CASSCF and MRCI methods, especially the later one, which incorporates both dynamical and nondynamical correlation effects, give results in good agreement with the experimental results. Both the experimental and accurate MRCI results indicate that the electronic ground state of FeO_2^- is a doublet spin state with a linear equilibrium geometry. Due to the strong spin-orbit coupling effect, excited electronic states are well separated from the electronic ground state and the later is barely affected by the Renner-Teller and pseudo-Jahn-Teller effects. One would expect that other isoelectronic molecules, such as FeS_2^- ,⁶⁹ RuO_2^- , CoO_2 ,^{27,29} RhO_2 , NiO_2^+ , PdO_2^+ , and PtO_2^+ ,³⁰ may also have similar linear electronic ground states. As mentioned in the Introduction section, experimental evidence indeed indicates that CoO_2 is a linear molecule with a doublet ground state and multireference methods predict a linear PtO_2^+ with a doublet ground state. Thus theoretical calculations involving these molecules with use of post-HF methods and DFT methods might be unreliable. Further studies on these interesting metal compounds are suggested.

Acknowledgment. This work is supported by National Basic Research Program of China (2004CB719501 and 2007CB815203)

and the National Natural Science Foundation of China (20673024 and 20773030).

References and Notes

- Bagus, P. S.; Preston, H. J. *J. Chem. Phys.* **1972**, *59*, 2986.
- Abramowitz, S.; Acquista, N.; Levin, I. W. *Chem. Phys. Lett.* **1977**, *50*, 423.
- Green, D. W.; Reedy, G. T.; Kay, J. G. *J. Mol. Spectrosc.* **1979**, *78*, 257.
- Chang, S.; Blyholder, G.; Fernandez, J. *Inorg. Chem.* **1981**, *20*, 2813.
- Cheung, A. S. C.; Gordon, R. M.; Merer, A. J. *J. Mol. Spectrosc.* **1981**, *87*, 289. Steimle, T. C.; Nachman, D. F.; Shirley, J. E.; Merer, A. J. *J. Chem. Phys.* **1989**, *90*, 5360.
- Krauss, M.; Stevens, W. J. *J. Chem. Phys.* **1985**, *82*, 5584.
- Bauschlicher, C. W., Jr.; Langhoff, S. R.; Komornicki, A. *Theor. Chim. Acta* **1990**, *77*, 263. Bauschlicher, C. W., Jr.; Maitre, P. *Theor. Chim. Acta* **1995**, *90*, 189.
- Fanfarillo, M.; Downs, A. J.; Green, T. M.; Almond, M. J. *Inorg. Chem.* **1992**, *31*, 2973.
- Lyne, P. D.; Mingos, D. M. P.; Ziegler, T.; Downs, A. J. *Inorg. Chem.* **1993**, *32*, 4785.
- Schröder, D.; Fiedler, A.; Schwarz, J.; Schwarz, H. *Inorg. Chem.* **1994**, *33*, 5094.
- Andrews, L.; Chertihin, G. V.; Ricca, A.; Bauschlicher, C. W., Jr. *J. Am. Chem. Soc.* **1996**, *118*, 467. Chertihin, G. V.; Saffel, W.; Yustein, J. T.; Andrews, L.; Neurock, M.; Ricca, A.; Bauschlicher, C. W., Jr. *J. Phys. Chem.* **1996**, *100*, 5261.
- Schröder, D.; Schwarz, H.; Shaik, S. *Struct. Bonding (Berlin)* **2000**, *97*, 91.
- Yamada, Y.; Sumino, H.; Okamura, Y.; Shimasaki, H.; Tominaga, T. *Appl. Radiat. Isot.* **2000**, *52*, 157.
- Uzunova, E. L.; St. Nikolov, G.; Mikosch, H. *ChemPhysChem* **2004**, *5*, 192.
- Engelking, P. C.; Lineberger, W. C. *J. Chem. Phys.* **1977**, *66*, 5054. Andersen, T.; Lykke, K. R.; Neumark, D. M.; Lineberger, W. C. *J. Chem. Phys.* **1987**, *86*, 1858.
- Fan, J.; Wang, L. S. *J. Chem. Phys.* **1995**, *102*, 8714.
- (a) Wu, H. B.; Desai, S. R.; Wang, L. S. *J. Am. Chem. Soc.* **1996**, *118*, 5296. (b) Wu, H. B.; Desai, S. R.; Wang, L. S. *J. Am. Chem. Soc.* **1996**, *118*, 7434. (c) Wang, L. S.; Wu, H. B.; Desai, S. R. *Phys. Rev. Lett.* **1996**, *76*, 4853.
- Self, D. E.; Plane, M. C. *Phys. Chem. Chem. Phys.* **2003**, *5*, 1407.
- Shiroishi, H.; Oda, T.; Hamada, I.; Fujima, N. *Mol. Simul.* **2004**, *30*, 911. Shiroishi, H.; Oda, T.; Hamada, I.; Fujima, N. *Polyhedron* **2005**, *24*, 2472.
- Reilly, N. M.; Reveles, J. U.; Johnson, G. E.; Khanna, S. N.; Castleman, A. W., Jr. *J. Phys. Chem. A* **2007**, *111*, 4158.
- Blyholder, G.; Head, J.; Ruetter, F. *Inorg. Chem.* **1982**, *21*, 1539.
- Cao, Z. X.; Duran, M.; Sola, M. *Chem. Phys. Lett.* **1997**, *274*, 411.
- Gutsev, G. L.; Khanna, S. N.; Rao, B. K.; Jena, P. *J. Phys. Chem. A* **1999**, *103*, 5812.
- Gutsev, G. L.; Rao, B. K.; Jena, P. *J. Phys. Chem. A* **2000**, *104*, 11961.
- Cao, Z.; Wu, W.; Zhang, Q. *J. Mol. Struct. (THEOCHEM)* **1999**, *489*, 165.
- García-Sosa, A. T.; Castro, M. *Int. J. Quantum Chem.* **2000**, *80*, 307.
- Chertihin, G. V.; Citra, A.; Andrews, L.; Bauschlicher, C. W., Jr. *J. Phys. Chem. A* **1997**, *101*, 8793. Danset, D.; Alikhani, M. E.; Manceron, L. *J. Phys. Chem. A* **2005**, *109*, 97.
- Uzunova, E. L.; Nikolov, G. S.; Mikosch, H. *J. Phys. Chem. A* **2002**, *106*, 4104.
- Van Zee, R. J.; Hamrick, Y. M.; Li, S.; Weltner, W., Jr. *J. Phys. Chem.* **1992**, *96*, 7247.
- Brönstrup, M.; Schröder, D.; Kretzchmar, I.; Schwarz, H.; Harvey, J. N. *J. Am. Chem. Soc.* **2001**, *123*, 142.
- Wang, G. J.; Zhou, M. F. *Int. Rev. Phys. Chem.* **2008**, *27*, 1. Zhou, M. F.; Tsumori, N.; Xu, Q.; Kushto, G. P.; Andrews, L. *J. Am. Chem. Soc.* **2003**, *125*, 11371. Wang, G. J.; Gong, Y.; Chen, M. H.; Zhou, M. F. *J. Am. Chem. Soc.* **2006**, *128*, 5974.
- Head-Gordon, M.; Pople, J. A.; Frisch, M. J. *Chem. Phys. Lett.* **1988**, *153*, 503. Frisch, M. J.; Head-Gordon, M.; Pople, J. A. *Chem. Phys. Lett.* **1990**, *166*, 275.
- Pople, J. A.; Seeger, R.; Krishnan, R. *Int. J. Quantum Chem. Symp.* **1976**, *10*, 1. Pople, J. A.; Seeger, R.; Krishnan, R. *Int. J. Quantum Chem. Symp.* **1977**, *11*, 149.
- Krishnan, R.; Pople, J. A. *Int. J. Quantum Chem.* **1978**, *14*, 91.
- Cizek, J. *Adv. Chem. Phys.* **1969**, *14*, 35. Purvis, G. D.; Bartlett, R. J. *J. Chem. Phys.* **1982**, *76*, 1910. Scuseria, G. E.; Janssen, C. L.; Schaefer, H. F., III. *J. Chem. Phys.* **1988**, *89*, 7382. Scuseria, G. E.; Schaefer, H. F., III. *J. Chem. Phys.* **1989**, *90*, 3700.

- (36) Bartlett, R. J.; Purvis, G. D. *Int. J. Quantum Chem.* **1978**, *14*, 516.
Krishnan, R.; Pople, J.; Schlegel, H. B.; Binkley, J. S. *Int. J. Quantum Chem.* **1978**, *14*, 545.
- (37) Becke, A. D. *Phys. Rev. A* **1988**, *38*, 3098.
- (38) Lee, C.; Yang, W.; Parr, R. G. *Phys. Rev. B* **1988**, *37*, 785.
- (39) Handy, N. C.; Cohen, A. J. *Mol. Phys.* **2001**, *99*, 403.
- (40) Perdew, J. P. In *Electronic Structure of Solids '91*; Ziesche, P.; Esching, H., Eds.; Akademie Verlag: Berlin, Germany, 1991; p 11.
- (41) Wilson, P. J.; Bradley, T. J.; Tozer, D. J. *J. Chem. Phys.* **2001**, *115*, 9233.
- (42) Hoe, W.-M.; Cohen, A. J.; Handy, N. C. *Chem. Phys. Lett.* **2001**, *341*, 319.
- (43) Stephens, P. J.; Devlin, F. J.; Chabalowski, C. F.; Frisch, M. J. *J. Phys. Chem.* **1994**, *98*, 11623.
- (44) Becke, A. D. *J. Chem. Phys.* **1993**, *98*, 5648.
- (45) Tao, J.; Perdew, J. P.; Staroverov, V. N.; Scuseria, G. E. *Phys. Rev. Lett.* **2003**, *91*, 146401.
- (46) Adamo, C.; Barone, V. *Chem. Phys. Lett.* **1997**, *274*, 242.
- (47) Becke, A. D. *J. Chem. Phys.* **1993**, *98*, 1372.
- (48) Frisch, M. J.; Trucks, G. W.; Schlegel, H. B.; Scuseria, G. E.; Robb, M. A.; Cheeseman, J. R.; Montgomery, J. A., Jr.; Vreven, T.; Kudin, K. N.; Burant, J. C.; Millam, J. M.; Iyengar, S. S.; Tomasi, J.; Barone, V.; Mennucci, B.; Cossi, M.; Scalmani, G.; Rega, N.; Petersson, G. A.; Nakatsuji, H.; Hada, M.; Ehara, M.; Toyota, K.; Fukuda, R.; Hasegawa, J.; Ishida, M.; Nakajima, T.; Honda, Y.; Kitao, O.; Nakai, H.; Klene, M.; Li, X.; Knox, J. E.; Hratchian, H. P.; Cross, J. B.; Adamo, C.; Jaramillo, J.; Gomperts, R.; Stratmann, R. E.; Yazyev, O.; Austin, A. J.; Cammi, R.; Pomelli, C.; Ochterski, J. W.; Ayala, P. Y.; Morokuma, K.; Voth, G. A.; Salvador, P.; Dannenberg, J. J.; Zakrzewski, V. G.; Dapprich, S.; Daniels, A. D.; Strain, M. C.; Farkas, O.; Malick, D. K.; Rabuck, A. D.; Raghavachari, K.; Foresman, J. B.; Ortiz, J. V.; Cui, Q.; Baboul, A. G.; Clifford, S.; Cioslowski, J.; Stefanov, B. B.; Liu, G.; Liashenko, A.; Piskorz, P.; Komaromi, I.; Martin, R. L.; Fox, D. J.; Keith, T.; Al-Laham, M. A.; Peng, C. Y.; Nanayakkara, A.; Challacombe, M.; Gill, P. M. W.; Johnson, B.; Chen, W.; Wong, M. W.; Gonzalez, C.; Pople, J. A. *Gaussian 03*, Revision B.05; Gaussian, Inc.: Pittsburgh, PA, 2003.
- (49) Schultz, N. E.; Zhao, Y.; Truhlar, D. G. *J. Phys. Chem. A* **2005**, *109*, 4388. Zhao, Y.; Truhlar, D. G. *J. Chem. Phys.* **2006**, *124*, 224105. Zhao, Y.; Truhlar, D. G. *J. Chem. Phys.* **2006**, *125*, 194101. Schultz, N. E.; Gherman, B. F.; Cramer, C. J.; Truhlar, D. G. *J. Phys. Chem. B* **2006**, *110*, 24030.
- (50) Schultz, N. E.; Zhao, Y.; Truhlar, D. G. *J. Phys. Chem. A* **2005**, *109*, 11127.
- (51) Hegarty, D.; Robb, M. A. *Mol. Phys.* **1979**, *38*, 1795. Eade, R. H. E.; Robb, M. A. *Chem. Phys. Lett.* **1981**, *83*, 362. Schlegel, H. B.; Robb, M. A. *Chem. Phys. Lett.* **1982**, *93*, 43. Bernardi, F.; Bottini, A.; McDougall, J. J. W.; Robb, M. A.; Schlegel, H. B. *Faraday Symp. Chem. Soc.* **1984**, *19*, 137.
- (52) Burton, P. G.; Buenker, R. J.; Bruna, P. J.; Peyerimhoff, S. D. *Chem. Phys. Lett.* **1983**, *95*, 379. Bauschlicher, C. W., Jr.; Taylor, P. R. *J. Chem. Phys.* **1987**, *86*, 858. Shavitt, I.; Brown, F. B.; Burton, P. G. *Int. J. Quantum Chem.* **1987**, *31*, 507.
- (53) Balabanov, N. B.; Peterson, K. A. *J. Chem. Phys.* **2005**, *123*, 064107.
- (54) Douglas, M.; Kroll, N. M. *Ann. Phys. (NY)* **1974**, *82*, 89. Hess, B. A. *Phys. Rev. A* **1986**, *33*, 3742.
- (55) Werner, H.-J.; Knowles, P. J.; Lindh, R. et al. *MOLPRO*, version 2002.6, a package of ab initio programs; University College Cardiff Consultants Limited, 2003.
- (56) Bondybey, V. E.; Smith, A. M.; Argreiter, J. *Chem. Rev.* **1996**, *96*, 2113.
- (57) Chertihin, G. V.; Andrews, L. *J. Chem. Phys.* **1998**, *108*, 6404. Zhou, M. F.; Hacıoglu, J.; Andrews, L. *J. Chem. Phys.* **1999**, *110*, 9450. Dong, J.; Wang, Y.; Zhou, M. F. *Chem. Phys. Lett.* **2002**, *364*, 511.
- (58) Gong, Y.; Zhou, M. F.; Andrews, L. *J. Phys. Chem. A* **2007**, *111*, 12001.
- (59) Zhao, Y. Y.; Gong, Y.; Zhou, M. F. *J. Phys. Chem. A* **2006**, *110*, 10777.
- (60) Zhou, M. F.; Andrews, L. *J. Am. Chem. Soc.* **1998**, *120*, 11499.
- (61) Scott, A. P.; Radom, L. *J. Phys. Chem.* **1996**, *100*, 16502. Zheng, J.; Lynch, B. J.; Zhao, Y.; Truhlar, D. G. Database of Frequency Scaling Factors for Electronic Structure Methods, 2007, available online at http://comp.chem.umn.edu/database/freq_scale.htm.
- (62) Cohen, R. D.; Sherrill, C. D. *J. Chem. Phys.* **2001**, *114*, 8257.
- (63) Sherrill, C. D.; Lee, M. S.; Head-Gordon, M. *Chem. Phys. Lett.* **1999**, *302*, 425. Dunietz, B. D.; Head-Gordon, M. *J. Phys. Chem. A* **2003**, *107*, 9160.
- (64) Lee, T. J.; Taylor, P. R. *Int. J. Quantum Chem. Symp.* **1989**, *23*, 199.
- (65) Russ, N. J.; Crawford, T. D.; Tschumper, G. S. *J. Chem. Phys.* **2004**, *120*, 7298.
- (66) Herzberg, G. *The Spectra and Structures of Simple Free Radicals: An Introduction to Molecular Spectroscopy*; Cornell University Press: Ithaca, NY, 1971.
- (67) Bersuker, I. B. *Chem. Rev.* **2001**, *101*, 1067.
- (68) Mishra, S.; Vallet, V.; Poluyanov, L. V.; Domcke, W. *J. Chem. Phys.* **2005**, *123*, 124104.
- (69) Zhai, H. J.; Kiran, B.; Wang, L. S. *J. Phys. Chem. A* **2003**, *107*, 2821.